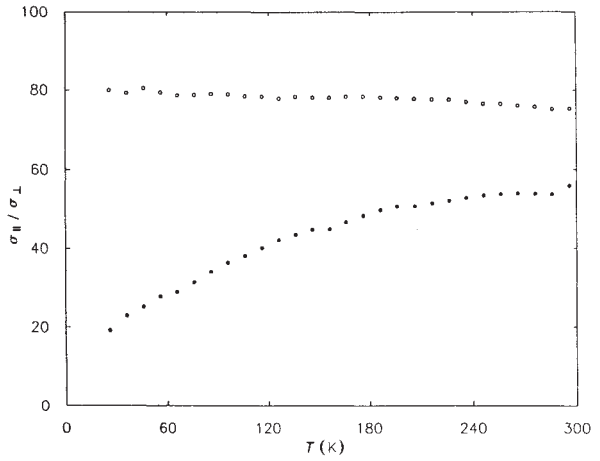

Fig. 4 Temperature dependence of $(\sigma_\parallel/\sigma_\perp)$ for pressures of 1 atm (solid dots) and 7 kbar (open circles); stretching ratio 6:1.

cally with time (down by about 30% over a period of a week) indicative of the irreversible degradation known for iodine doping[1,2].

Figure 2 shows the pressure dependence of $\sigma_\parallel$ at room temperature from 1 atm to 10 kbar. The parallel conductivity has a gentle maximum at about 7 kbar; the data are reversible on cycling up to 15 kbar. The perpendicular conductivity (not shown) increases by about 10% below 1 kbar and remains constant (within measurement error) at higher pressures. The pressure dependence of $\sigma_\parallel$ and $\sigma_\perp$ was checked on a number of different samples and found to be characteristic.

Figure 3 shows the temperature dependence of $\sigma_\parallel$ at several different pressures; high pressure suppresses the decrease in $\sigma_\perp(T)$ at low temperatures. This effect is emphasized in the inset to Fig. 3 where we plot the ratio $[\sigma_\parallel(7\text{ kbar})/\sigma_\parallel(1\text{ atm})]$ as a function of temperature.

The anisotropy of the conductivity is relatively large compared to that obtained from previous measurements on material prepared by the Shirakawa method; we find $(\sigma_\parallel/\sigma_\perp) \approx 80$ at 7 kbar. The anisotropy is somewhat higher at high pressure, as $\sigma_\parallel$ increases with pressure while $\sigma_\perp$ remains essentially constant. The temperature dependence of $(\sigma_\parallel/\sigma_\perp)$ is shown in Fig. 4 for pressures of 1 atm and 7 kbar. Note that at high pressure, the ratio is constant.

The observation of a temperature- and pressure-dependent anisotropy suggests that the transport data are beginning to provide information on intrinsic processes. The magnitude and temperature independence of $\sigma_\parallel(T)$ below 1 K implies genuine metallic behaviour for heavily doped polyacetylene (consistent with specific heat[6], thermopower[7] and susceptibility data[8]) and rules out transport by hopping among strongly localized states. Note, however, that $\sigma_\parallel(T)$ increases with increasing temperature implying that phonon-assisted transport (either through microscopic localized states or across inter-fibrillar barriers) is involved. Thus, although this modified synthesis yields significantly higher-quality polyacetylene (with $\sigma_\parallel$ within about a factor of 20 of the conductivity of copper) the transport is still limited by material imperfection.

Although improvement of solid-state properties through higher-quality materials is a general feature of materials science, there has been little optimism that this rule would be applicable to conducting polymers. Perhaps the reason for this was the argument that the high level of impurities in doped conducting polymers would negate any improvements towards molecular chain perfection. The present study demonstrates that this is not the case in polyacetylene or (by implication) in other conducting polymers: the achievement of still higher-quality material from improved synthesis and processing can be expected to lead to correspondingly better electronic properties.

The research at UCSB was supported by the Office of Naval Research.

Note added in proof: H.N. recently announced further improvements in the preparation of oriented polyacetylene leading to a room temperature electrical conductivity of $\sim 1.5 \times 10^{+5}$ S cm^{-1} with an anisotropy of $\sim 10^3$ (*American Chemical Society Meeting Symposium on Conducting Polymers, Their Emergence and Future*; April 7-8, 1987, Denver, Colorado).

Received 3 February; accepted 23 March 1987.

1. Skotheim, T. J. (ed.) *Handbook of Conducting Polymers* (ed. Skotheim, T. J.) (Dekker, New York, 1986).
2. Etemad, S., Heeger, A. J. & MacDiarmid, A. G. *A. Rev. Phys. Chem.* **33**, 443 (1982).
3. Gould, C. M. *et al. Phys. Rev.* B **23**, 6820 (1981).
4. Shirakawa, H. & Ikeda, S. *Synth. Met.* **1**, 175 (1980).
5. Naarmann, H. *Synth. Met.* **17**, 223 (1987).
6. Moses, D., Denenstein, A., Pron, A., Heeger, A. J. & MacDiarmid, A. G. *Solid St. Commun.* **36**, 219 (1980).
7. Park, Y. W., Denenstein, A., Chiang, C. K., Heeger, A. J. & MacDiarmid, A. G. *Solid St. Commun.* **29**, 747 (1979).
8. Moraes, F., Chen, J., Chung, T.-C. & Heeger, A. J. *Synth. Met.* **11**, 271 (1985).

Lightning triggered from the Earth's magnetosphere as the source of synchronized whistlers

W. C. Armstrong

STARLAB, 324 Durand Building, Stanford University, Stanford, California 94305, USA

Specific patterns established by natural radio signals echoing periodically in a magnetospheric whistler duct[1-3] are sometimes observed to indicate strongly preferred times at which identical, well-defined whistlers occur. Ordinarily such whistlers would be assumed to originate in the stronger ground strokes[4] of spontaneous lightning. These nonrandom whistlers are therefore unexpected and raise the possibility that some whistler-source discharges may be triggered from the magnetosphere. The same possibility could also be predicted independently from another type of our recent observations. Selected examples of nonrandom whistlers are given here and the supporting observations described. In the absence of a previously developed theoretical explanation, a trigger mechanism is outlined which emphasizes discontinuous discharge to the upper atmosphere[5]. Such a mechanism might help explain several related phenomena.

Examples to be shown are from Southern Hemisphere data recorded at Siple Station, Antarctica, 76° S, 84° W geographic. Two nearly identical whistlers W_1 and W_2 occur in Fig. 1, each arriving about two seconds after its Northern Hemisphere source discharge. The second (W_2) is approximately in phase with echoes due to the first (W_1). If many whistlers were found with phasing identical to W_2, then their source discharges could no longer be thought of as spontaneous. Here, solid diagonal lines repeat a base period measured near 3.0 kHz between the leading edges of W_1 and its 'two-hop echo', e_1.

Because they are quickly eroded by path-propagation losses, successive echoes e_1-e_5 weaken and collapse toward a single frequency. This illustrates two important points: first, if periodic signals are to continue echoing in a long train, supplemental energy usually is required and second, if a unique period is maintained, it is usually because of a dominant signal echoing at a single frequency. Here 'echo' E_2 shows supplemental energy mostly at constant frequency. The starting time of E_2 shows that the leading edge of W_1 has established the periodicity.

With energy now being added, each echo grows gradually and becomes more complex until E_5 (not labelled) and supplemental emission T_2 result. W_2 appears to follow precisely in phase with T_2, so a Northern Hemisphere source discharge might be triggered in connection with T_2's northern reflection.

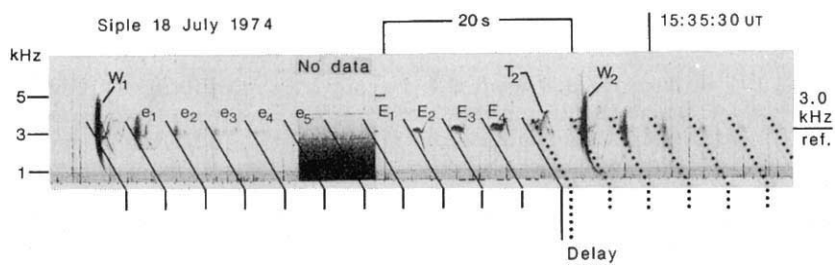

Fig. 1 A sequence of echoes (e_1–e_5) started by a previous whistler (W_1), later shows supplemental energy in the form of emissions E_1–E_5 (E_5 not labelled) and T_2. A whistler (W_2) then follows approximately in phase. Solid and dotted lines indicate uniform periodicity, measured at about 3.0 kHz. Delay is discussed in the text. Note how W_2 'falls on top of' the weak emission E_6 (not labelled). This specific configuration, whistler 'on top of' an emission, has characterized probable triggered whistlers like W_2 in about ten other echo sequences found to date. An example appears as Fig. 1 of ref. 1.

However, in the cases studied to date, whistlers like W_2 are more consistently associated with stimulation and more gradual (therefore more delayed) growth of signal energy, such as that supplementing the echoes at nearly constant frequency. With respect to the start of E_5, delay of about 27% of the base period near 3.0 kHz is passed on to W_2 and its echoes, which then maintain the original periodicity (dotted lines). Such delay is probably due to several aspects of the triggering process.

Two other examples (not shown) of whistlers in patterns identical to that of Fig. 1 were recorded on 21 March 1977 at Roberval, Quebec, Canada near the northern end of the Siple geomagnetic field line. These examples are significant because they show the whistler source-stroke sferics (radio impulses). These are prominent, but not otherwise extraordinary, for each whistler, whether spontaneous or triggered.

Nonrandom whistlers also occur in less transient, more steady-state situations. For example, with supplemental energy apparently drawn from a band of hiss (Fig. 2), uniform echoing remains evident during trains which are longer and less dependent on regeneration (extension) by any single synchronized whistler. Such whistlers are seen to be numerous and very similar however, probably because long echo trains provide more opportunity for regular occurrence and for repeated identification. As the first 'echoes' become established, their separation may increase by as much as 10% to match that of the synchronous whistlers. Compared to the first example given, both stimulation of echoes from hiss and triggering of whistlers appear to be more continuous and simultaneously under periodic control which is quite stable. The six synchronized whistlers in Fig. 2 are spread over an unusually long train of 59 echoes. Two different whistlers (W_3 and W_7) have identical echoes separated by $N = 37$ intervals, so the average interval can be measured with ±0.3% accuracy. It is within 4% of the basis of spacing of all the whistlers and identically equal to the basis of spacing of the whistlers W_3, W_5 and W_7 which are within ±0.25% of perfect periodicity. Note that anomalous W_6 timing is to be expected because W_5 has no opportunity to echo. Taking the worst-case irregularity of the period to be equivalent to the poor (phase) definition of individual echoes, a simple estimate gives a maximum probability of 1/15,625 that all six whistlers are independent random events.

Other observations independently suggest the existence of discharges triggered from the magnetosphere. First, a type of radio reflection change[6] thought to register a perturbation of electron density at ionospheric D-region altitudes, sometimes occurs very impulsively in about 50 ms[7,8], possibly indicating charge redistribution at ten or more times the normal rate. Since this rise time is about that of transient ionization columns detected by radar[9], both types of event might involve similarly impulsive currents enduring about as long as some lightning flashes[10]. Lightning (predominantly simultaneous) has been clearly indicated with each of about 25 impulsive reflection change events studied to date.

In a second case, significant, impulsive reflection changes (with sferics) occurred selectively at the times of energetic, radiation-belt electron bursts detected independently during precipitation into the ionosphere[11]. Impulsive changes were observed only with some of the bursts, so it seems likely that an impulsive current or other possible cause[43], perhaps including simultaneous lightning, was triggered by particular bursts.

Third, these same electron bursts were repeatedly correlated with whistlers and characteristic emissions[11] indicating pitch-angle scattering of magnetospheric electrons as the source of a burst[12,13]. Furthermore, the emissions were a type previously indicative of bremsstrahlung X-ray bursts energetic enough to be detected at 30-km (7g cm^{-2}) balloon altitude[14]. If we could show that such X-ray bursts sometimes trigger discharges which produce new whistlers, then we would predict the occurrence of nonrandom whistlers similar to the examples given here. We now discuss this possibility.

With other analyses or reports[15–25] of similarly impulsive and/or synchronized behaviour, the evidence given above suggests a common mechanism as follows. On rare occasions, charge lowered to earth by a spontaneous lightning flash is immediately replaced by an impulsive current which taps a source sometimes as high as ionospheric altitude. Conversely, sometimes a stroke to ground immediately removes charge lowered by a spontaneous impulsive current which partially neutralizes the top of a tropospheric charge dipole. Such currents probably require temporary 'filaments' of enhanced conductivity to be formed in advance. Conditions affecting filament formation, particularly their length, continuity, and number determine which macroscopic phenomena occur. Energy is supplied primarily from the charge dipole.

One type of conductive filament which could actively conform to a path of minimum potential difference might be formed by a string of 'bubbles' even if these carried no net electrical charge[26]. Formation might begin when a physical 'phase change' initiates local 'electrical boiling'[27,28] in the lower atmosphere. Just as ordinary boiling indicates heat flow greater than free or organized[29,30] convection can support, the transition to electrical boiling would mean that electrostatic 'leakage' currents are otherwise unable to transfer charge at the higher net rate required by other processes. On a smaller scale, the transition to a (very stable) organized[30] state similar to a string of (higher altitude) 'bubbles' might be said to occur when increasing voltage produces luminous structures in a low-pressure laboratory gas-discharge tube. Analogously, we are discussing a physical regime which temporarily produces a steady-state charge distribution having no time to relax, in the atmospheric example, to that of an equilibrium electrosphere[31].

An assumption of local electrical phase change means that electrostatic (equilibrium) computational models can be expected to approximate correctly only those (steady-state) parts of the actual behaviour which remain nearly electrostatic. The following preliminary analysis is therefore somewhat fragmentary, perhaps like a series of snapshots.

Starting with 3,000 bubbles $10 \times 10 \times 10$ m^3 formed at 1 bubble per second and spaced 10 m apart, we find that it takes 100 min to fill a 60-km column. Assume a field 0.3 kV m^{-1} (breakdown) at 70 km and a spherical bubble of radius r carrying (negative) 1/25 mC (downward). This gives 0.12 C on the filament. If viscous drag is to hold the (formation) velocity to 10 ms^{-1}, then by Stokes Law, the radius r is about 4 m. Note that 1/25 mC on a 600-m^2 bubble produces 7.5 kV m^{-1}, breakdown at about 42 km. Above that, such (transient) bubbles are 'overcharged'.

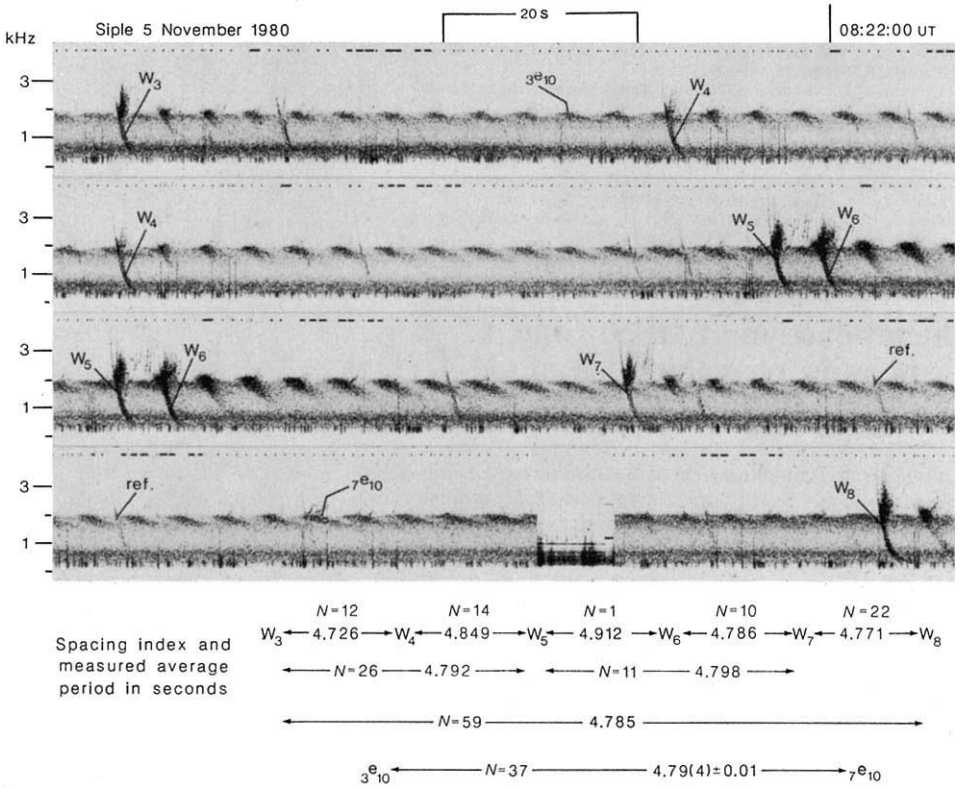

Fig. 2 Whistler 'echoes' form long trains apparently by drawing energy from a band of hiss. Each panel overlaps the one below it and some whistlers are shown twice for continuity. Whistlers and echoes have the same average periodicity throughout. Typical measurement accuracy of a whistler's position is ±12 ms, made possible by some well-defined whistler segments. These whistlers travelled a path intersecting the Earth's surface in central Quebec, Canada at about 53° N geographic. A high-latitude winter storm is therefore implied, for which a model study finds coupling to the ionosphere possibly more significant[41]. Several weaker whistlers having accurate $N+1/2$ phases could be due to a different kind of triggering. An event of this clarity, having just enough whistlers to make synchronization obvious, probably requires unusual matching between magnetospheric echoing and (cloud) charge-separating conditions. We estimate (very roughly) five or fewer such events a year worldwide.

We will assume the inconsistency means that the region 40–70 km is actually one of forced, electrical convection irregularities[32] or vortices and scale-size reduction producing charge and field concentration[33,34].

Should electrostatic repulsion increase the bubble radius a factor of 3.3 during transit, limiting sonic velocity 300 ms^{-1} would occur in a 30 $kV\,m^{-1}$ breakdown field at about 35 km. Also, with 1,000 MV[5,35] cloud-ionosphere potential spread equally over 10-m gaps between 3,000 bubbles, we find breakdown is exceeded at a similar altitude. As these two views apparently have a similar limitation, we assume that a temporary charge layer could form at 35 km. This might explain a large decay time constant in one set of observations[7,8]. Above 35 km, a steady-state filament may be more like the indefinitely extendable positive column of a gas discharge[36], with sonic velocities or other departure from equilibrium limited by oscillation.

A charge layer at (say) 30-km altitude would have about 0.5 C km^{-2} if it shielded 0.3 $kV\,m^{-1}$ above from 60 $kV\,m^{-1}$ below. If the layer is 3 km thick, the excess charge density is about 100 times that typical at 70 km for (presumed) electrostatic equilibrium. This could give 900 MV at 60 $kV\,m^{-1}$ across the lower 15 km and 12 MV at 0.3 $kV\,m^{-1}$ across the upper 40 km. Now, if conduction avalanches along the upper part of the filament, the lower 900 MV could jump suddenly (in 20 ms) by more than 10%, possibly causing electron runaway and X rays[37] to complete the breakdown with upward lightning[17–25].

Because it is a good source of ionizing bremsstrahlung X-ray bursts which have been observed to penetrate to 30 km altitude[14], the magnetosphere is actually a quite plausible trigger source in this situation. Delay between the start of a synchronous 'echo' (Figs 1 and 2) and any triggered whistler is probably due mostly to the magnetospheric processes[12,14,38].

Many other details considered in terms of the current statement of the problem also recommend a type of phase-change explanation. The extent of any departure from equilibrium is a primary question. Reference 9 gives insight into the history of the topic. A positive column structure[36] may be an essential feature, and its triggering could play a more general role, for example in 'sympathetic' lightning[39] or as a supplement to solar ionization in Sun–weather coupling[35,40].

The author thanks his colleagues for their help and the NSF Division of Polar Programs for support.

Note added in proof. There exists a model[42], previously unknown to the author, which extends Wilson's picture[5] somewhat; another view[43] suggests how phase changes in the electrical medium, possibly of central importance to some observations[6–9,16], might occur in the atmosphere. Also, some experiments[44] have shown how discharges may respond to space-charge 'bubbles'.

Received 19 May 1986; accepted 18 March 1987.

1. Helliwell, R. A. & Brice, N. *J. geophys. Res.* **69**, 4704–4708 (1964).
2. Bernhardt, P. A. & Park, C. G. *J. geophys. Res.* **82**, 5222–5230 (1977).
3. Helliwell, R. A. *Whistlers and Related Ionospheric Phenomena* (Stanford University Press, 1965).
4. Norinder, H. & Knudsen, E. *Planet. Space Sci.* **1**, 173–183 (1959).
5. Wilson, C. T. R. *Proc. Phys. Soc.* **37**, 32D–37D (1925).
6. Carpenter, D. L., Inan, U. S., Trimpi, M. L., Helliwell, R. A. & Katsufrakis, J. P. *J. geophys. Res.* **89**, 9857–9862 (1984).
7. Armstrong, W. C. *Antarct. J. U.S.* **18**, 281–283 (1983).
8. Armstrong, W. C. & Carpenter, D. L. *Eos* **63**, 1071 (1982).
9. Rumi, G. C. *J. geophys. Res.* **62**, 547–564 (1957).
10. Uman, M. A. & Krider, E. P. *IEEE Trans. electromagn Compat* **24**, 79–112 (1982).
11. Armstrong, W. C. *et al. Eos* **65**, 1061 (1984); *Eos* **64**, 815 (1983).
12. Helliwell, R. A., Mende, S. B., Doolittle, J. H., Armstrong, W. C. & Carpenter, D. L. *J. geophys. Res.* **85**, 3376–3386 (1980).
13. Rycroft, M. *J. planet. Space Sci.* **21**, 239–251 (1973).
14. Rosenberg, T. J. *et al. J. geophys. Res.* **86**, 5819–5832 (1981).
15. Cole, R. K. Jr, Hill, R. D. & Pierce, E. T. *J. geophys. Res.* **71**, 959–964 (1966).
16. Isted, G. A. *Marconi Rev.* **17**, 37–60 (1954).
17. Boys, C. V. *Nature* **118**, 749–750 (1926).
18. Malan, D. J. *C.r. hebd. Séanc. Acad. Sci., Paris* **205**, 812–813 (1937).
19. Wright, J. B. *Weather* **5**, 230 (1950).
20. Ashmore, S. E. *Weather* **5**, 331 (1950).
21. Hoddinott, M. H. O. *Weather* **5**, 331 (1950).
22. Wood, C. A. *Weather* **6**, 64 (1951).
23. Vonnegut, B. *Weather* **35**, 59–60 (1980).
24. Schonland, B. F. J. *The Flight of Thunder-bolts* 50–51 (Clarendon, Oxford, 1964).
25. Vaughn, O. H., Jr. & Vonnegut, B. *Weatherwise* **35**, 70–72 (1982).
26. Pohl, H. A. *J. appl. Phys.* **29**, 1182–1188 (1958).
27. Berezin, A. A. *J. Electrostat.* **18**, 193–197 (1986).
28. Nelson, J. K. & Hashad, I. F. M. *J. Electrostat.* **12**, 527–534 (1982).
29. Schmidt, R. J. & Milverton, S. W. *Proc. R. Soc.* **A152**, 586–594 (1935).
30. Nicholis, G. & Prigogine, I. *Self-organization in Non-equilibrium Systems* (Wiley, New York, 1977).
31. Israel, H. *Atmospheric Electricity* Vol. 1, 114–118 (US Department of Commerce, Springfield, Virginia, 1971).

32. Felici, N. J. *J. Electrostat.* **4**, 119-129 (1977).
33. Garton, C. G. & Krasucki, Z. *Proc. R. Soc.* **A280**, 211-226 (1964).
34. Wilson, C. T. R. & Taylor, G. I. *Proc. Camb. phil. Soc.* **22**, 728-730 (1925).
35. Markson, R. *Nature* **273**, 103-109 (1978).
36. Thomson, J. J. *Conduction of Electricity through Gasses* 2nd edn, 529-530 (Cambridge University Press, 1906).
37. McCarthy, M. & Parks, G. K. *Geophys. Res. Lett.* **12**, 393-396 (1985).
38. Park, C. G. & Helliwell, R. A. *J. geophys. Res.* **82**, 3634-3642 (1977).
39. Vonnegut, B. *Weather* **34**, 291 (1979).
40. Holzworth, R. H. & Mozer, F. S. *J. geophys. Res.* **84**, 363-367 (1979).
41. Nisbet, J. S. *J. geophys. Res.* **90**, 9831-9844 (1985).
42. Appleton, E. V. & Naismith, R. *Proc. Phys. Soc.* **45**, 389-398 appendix (1933).
43. Handel, P. H. *J. geophys. Res.* **90**, 5857-5863 (1985).
44. Williams, E. R., Cooke, C. M. & Wright, K. A. *J. geophys. Res.* **90**, 6059-6070 (1985).

The production of O(^{1}S) from dissociative recombination of O_2^+

Steven L. Guberman

Institute for Scientific Research, 33 Bedford Street, Lexington, Massachusetts 02173, USA and Harvard-Smithsonian Center for Astrophysics, 60 Garden Street, Cambridge, Massachusetts 02138, USA

The suggestion that the dissociative recombination (DR) of O_2^+ with an electron could be an important process in the Earth's upper atmosphere first appeared in the literature over 55 years ago[1]. In 1947, Bates and Massey[2] pointed out that DR of O_2^+ was the only process that could explain the observed electron recombination rates in the E and F1 regions of the ionosphere. In 1954, Nicolet[3] proposed that DR of O_2^+ was the source of the ionospheric emission at 5,577 Å in the Earth's airglow. In the intervening years, the DR of O_2^+ leading to O in the excited ^{1}S state has been the subject of several reviews and many papers[4,5] and has been termed the 'classical'[6] ionospheric source of the well-known green line emission. Nevertheless, the rate coefficient for DR leading to O(^{1}S) has never been reliably determined in the laboratory. Here, we report the first theoretical calculations of the rate coefficient for a wide range of temperatures.

The DR of O_2^+ with an electron leading to excited atomic oxygen in the ^{1}S state is described by

$$O_2^+ + e^- \rightarrow O + O(^1S) \quad (1)$$

For the low vibrational levels of the ion ($v < 10$), the products of reaction (1) can be described by a single potential energy curve of $^1\Sigma_u^+$ symmetry[7]. In agreement with earlier theoretical studies[7], analyses of the Atmosphere Explorer E satellite measurements have shown a correlation between the quantum yield of O(^{1}S) from reaction (1) and the extent of vibrational excitation of the ion although the vibrational distribution was unknown[8]. Dissociation on a surface leading to O(^{1}D)+O(^{1}S) has been supported by interferometer emission-line profile measurements at 5,577 Å taken by the Dynamics Explorer Satellite[9]. The modelling of this process requires knowledge of the dependence of the DR rate coefficients for production of ground and excited atoms on ion vibrational excitation and electron temperature. Except for the total DR rate coefficient to all channels[10-13], reliable rate coefficients and quantum yields leading to specific excited states of O from individual vibrational levels have not been previously available.

The mechanism[14] for DR is illustrated in Fig. 1. The ion in vibrational level v captures an electron of energy ε into a neutral repulsive state which can dissociate before the captured electron is emitted. The probability of capture into vibrational level v is proportional to a Franck-Condon (FC) factor between a bound ion vibrational wave function and a continuum wave function which has a small internuclear distance (R) turning point near the tip of the vertical arrow in Fig. 1. As ε increases, the turning point of the continuum wave function moves to smaller R, and the FC overlap samples the smaller R region of the bound ion wave function.

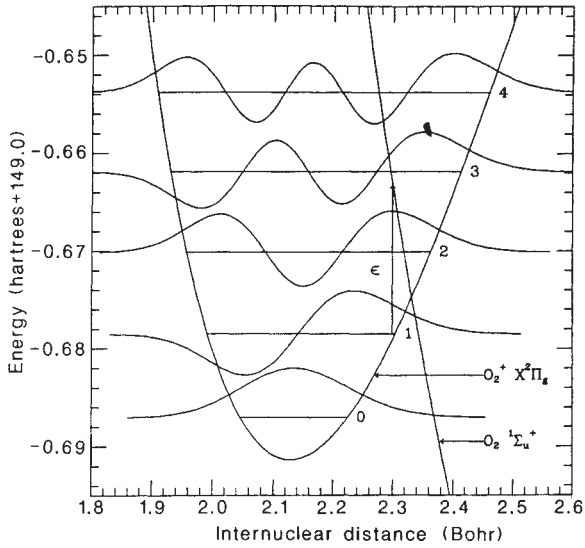

Fig. 1 Potential energy curves for the ground state of O_2^+ (from ref. 18) and for the dissociative $^1\Sigma_u^+$ state calculated here. The ion vibrational wave functions for the lowest five levels are each plotted on the same scale.

The orbitals for the large-scale wave functions reported here for the $^1\Sigma_u^+$ state have been determined in complete active space self-consistent field calculations (CASSCF)[15] over a nuclear-centred contracted gaussian basis set of *6s,3p,2d,1f* size. The final configuration interaction (CI) wave functions were expanded in terms of the CASSCF orbitals and generated from a ten-term reference set which contained all the configurations needed to describe the dissociation of $^1\Sigma_u^+$ to a ^{1}D and a ^{1}S oxygen atom. The CI involved all single and double excitations to the full virtual space and yielded a 139,946-term wave function. The SWEDEN group of programs (written by C. W. Bauschlicher, P. E. M. Siegbahn, B. Roos, P. Taylor and J. Almhof) and the direct CI method of Siegbahn were used to determine the large-scale wave functions[16]. The final energies, corrected for the missing quadruple excitations[17], were determined at 58 points in the range 1.85-8.0 a_0 (Bohr). The resulting potential curve for $^1\Sigma_u^+$ is shown in the region near the ion in Fig. 1. The ground-state ion potential curve is the RKR (Rydberg, Klein, Rees) curve[18] positioned at the experimental ionization potential above the calculated ground state and shifted by 0.0180 a_0 to larger R, to compensate for the difference between the calculated and experimental equilibrium R.

The cross-section, $\sigma(v)$, for DR through ion vibrational level v, was calculated using the expression derived by Giusti[19] in combination with numerically determined vibrational wave functions obtained by solving the one-dimensional nuclear Schrödinger equation in the $^1\Sigma_u^+$ and ion potentials. The cross-section is approximately directly proportional to an electronic width, Γ, which couples the electronic continuum of the free electron and ion to the repulsive dissociating resonance state. The width, a matrix element of the hamiltonian operator, is calculated using Fermi's Golden Rule. High principal quantum number Rydberg orbitals are determined in improved virtual orbital[20] calculations using an extended Rydberg basis set and are used to represent the free electron. The calculation of Γ is then a bound-state problem. The multi-configuration wave function for the ion plus high Rydberg orbital (or free electron) is optimized in the field of an optical potential in a procedure based on the use of Feshbach[21] projection operators (S.L.G., manuscript in preparation). Γ is determined for several values of the principal quantum number, n, of the Rydberg state and a threshold value is determined by extrapolating to $n \rightarrow \infty$. The resulting Γ calculated for the $^1\Sigma_u^+$ state of O_2 is 0.29 eV. The rate coefficient, α, is then obtained by averaging the cross-sections over a Maxwellian distribution of electron energies.